SLAC-PUB-14909

Submitted to ApJ Letters

Fermi Observations of GRB 090902B: A Distinct Spectral Component in the Prompt and Delayed Emission

Contact Authors:
Elisabetta Bissaldi (ebs@mpe.mpg.de), James Chiang (jchiang@slac.stanford.edu), Francesco de Palma (francesco.depalma@ba.infn.it), Sheila McBreen (smcbreen@mep.mpg.de)

on behalf of the *Fermi*/LAT and *Fermi*/GBM Collaborations

and *Swift* Team Members:
D. N. Burrows, V. d'Elia, P. W. A. Roming, G. Stratta, C. A. Swenson

ABSTRACT

We report on the observation of the bright, long gamma-ray burst, GRB 090902B, by the Gamma-ray Burst Monitor (GBM) and Large Area Telescope (LAT) instruments on-board the *Fermi* observatory. This was one of the brightest GRBs to have been observed by the LAT, which detected several hundred photons during the prompt phase. With a redshift of $z = 1.822$, this burst is among the most luminous detected by *Fermi*. Time-resolved spectral analysis reveals a significant power-law component in the LAT data that is distinct from the usual Band model emission that is seen in the sub-MeV energy range. This power-law component appears to extrapolate from the GeV range to the lowest energies and is more intense than the Band component both below ~ 50 keV and above 100 MeV. The Band component undergoes substantial spectral evolution over the entire course of the burst, while the photon index of the power-law component remains constant for most of the prompt phase, then hardens significantly towards the end. After the prompt phase, power-law emission persists in the LAT data as late as 1 ks post-trigger, with its flux declining as $t^{-1.5}$. The LAT detected a photon with the highest energy so far measured from a GRB, $33.4^{+2.7}_{-3.5}$ GeV. This event arrived 82 seconds after the GBM trigger and $\sim$50 seconds after the prompt phase emission had ended in the GBM band. We discuss the implications of these results for models of GRB emission and for constraints on models of the Extragalactic Background Light.

Subject headings: gamma rays: bursts

Work supported in part by US Department of Energy contract DE-AC02-76SF00515.

SLAC National Accelerator Laboratory, Menlo Park, CA 94025

1. Introduction

The *Fermi* Gamma-ray Space Telescope hosts two instruments, the Large Area Telescope (LAT, Atwood et al. 2009) and the Gamma-ray Burst Monitor (GBM, Meegan et al. 2009), which together are capable of measuring the spectral parameters of gamma-ray bursts (GRBs) across seven decades in energy. Since the start of GBM and LAT science operations in early August 2008, emission at energies >100 MeV has been detected from ten GRBs. Prior to *Fermi*, high-energy gamma-rays from GRBs with energies up to 18 GeV were observed by the EGRET instrument on-board the *Compton Gamma-ray Observatory*. The EGRET observations suggested three types of high-energy emission: an extrapolation of the low energy spectra to the >100 MeV band (e.g., Dingus et al. 1998), an additional spectral component during the prompt emission (González et al. 2003; Kaneko et al. 2008) and in the case of GRB 940217, a GeV afterglow which was detectable for 90 minutes after the trigger (Hurley et al. 1994). The redshifts of these events were not determined. Recently, Giuliani et al. (2008) reported that GRB 080514B which triggered AGILE at lower energies, was detected by the GRID instrument up to 300 MeV. A photometric redshift of $z = 1.8^{+0.4}_{-0.3}$ was reported for this event (Rossi et al. 2008).

In the *Fermi* era, due to the advanced localization capabilities of the LAT and the rapid follow-up by the *Swift* narrow field instruments (Gehrels et al. 2004) and the ground-based follow-up community, redshifts for five of the ten LAT bursts have been measured. These include GRB 080916C with $z = 4.35 \pm 0.15$ (Greiner et al. 2009), a long burst that has the highest inferred isotropic energy, $E_{\rm iso} \approx 8.8 \times 10^{54}$ ergs (10 keV–10 GeV) (Abdo et al. 2009d), and GRB 090510 with $z = 0.903 \pm 0.003$ (Rau et al. 2009), the second short burst seen by the LAT and the first short burst to show definitively an additional hard power-law component in the GeV band during the prompt phase (Abdo et al. 2009a).

GRB 090902B is a long, fairly intense burst with a redshift of $z = 1.822$ (Cucchiara et al. 2009) and fluence of $(4.36 \pm 0.06) \times 10^{-4}\,{\rm erg\,cm^{-2}}$ (10 keV–10 GeV) over the first 25 seconds of the prompt emission. These data give an isotropic energy $E_{\rm iso} = (3.63 \pm 0.05) \times 10^{54}$ ergs, comparable to that of GRB 080916C. Similar to GRB 090510, GRB 090902B has a significant additional, hard power-law component that appears during the prompt phase. However, unlike the earlier burst, a spectral feature at energies less than tens of keV is evident in the GBM spectrum of GRB 090902B that is consistent with an extrapolation of the >100 MeV power-law emission down to those energies.

We report on the observations and analysis of gamma-ray emission from GRB 090902B measured by the GBM and LAT instruments. In section 2, we present details of the detections by both instruments and summarize the follow-up observations. In section 3, we show the light curves of the prompt emission as seen by the various detectors and describe the extended

emission found in the LAT data out to 1 ks after the trigger. In section 4, we present the time-resolved spectral analysis of the burst emission during the prompt phase. Finally, in section 5, we discuss the physical interpretation of the GBM and LAT data, focusing in particular on the implications of the broad band power-law component for models of GRB physics.

2. Observations

On 2009 September 2 at 11:05:08.31 UT, the *Fermi* Gamma-ray Burst Monitor triggered on and localized the bright burst GRB 090202B (trigger 273582310 / 090902462, Bissaldi & Connaughton 2009). The burst was within the LAT field of view initially at an angle of 51° from the boresight. This event was sufficiently bright in the GBM that an Autonomous Repoint Request was made, and the spacecraft began slewing within 10 seconds towards the burst. After ∼200 seconds, it had pointed the LAT boresight to within a few degrees of the final burst localization. It maintained that pointing until ∼1 ks post-trigger, when the Earth's limb was starting to enter the LAT field-of-view (FOV). This burst was detected up to ∼5 MeV by GBM, and emission was significantly detected by the LAT, with 39 photons above 1 GeV (de Palma et al. 2009). The highest energy photon had $E = 33.4^{+2.7}_{-3.5}$ GeV and arrived 82 seconds after the GBM trigger; and the initial analyses detected photons as late as 300 seconds after the trigger (de Palma et al. 2009).

From the LAT data, the burst was localized to R.A.(J2000), Dec(J2000) = 265.00, 27.33 with a statistical uncertainty of 0.04° (+ <0.1° systematic) (de Palma et al. 2009), enabling Target of Opportunity observations to begin ∼12.5 hours after the trigger with the narrow field instruments on *Swift*. A candidate X-ray afterglow within the LAT error circle was detected by the X-Ray Telescope (XRT, Kennea & Stratta 2009). This source was confirmed to be fading (Stratta et al. 2009), and UVOT observations revealed the optical afterglow (Swenson & Siegel 2009; Swenson & Stratta 2009). The earliest ground-based optical observations were obtained by ROTSE-IIIa ∼1.4 hours post trigger (Pandey et al. 2009). Other detections were reported in the soft gamma-rays (Terada et al. 2009), in the optical (Perley et al. 2009; Guidorzi et al. 2009), in the near infrared by GROND (Olivares et al. 2009) and in the radio (van der Horst et al. 2009; Chandra & Frail 2009). The location of the fading source detected by GROND was R.A.(J2000), Dec(J2000) = $17^{\rm h}39^{\rm m}45\overset{\rm s}{.}41$, $+27°19'27.1''$, 3.3 arcminutes from the LAT location (Olivares et al. 2009). The afterglow redshift of $z = 1.822$ was measured by Cucchiara et al. (2009) using the GMOS spectrograph mounted on the Gemini-North telescope.

3. Light Curves

In Figure 1, we show the GBM and LAT light curves in several energy bands. The top three panels show data from the most brightly illuminated NaI and BGO detectors of the GBM, and the bottom three panels show the LAT data with various event selections. In the bottom panel, the measured photon energies are plotted as a function of time, including the highest energy event ($E = 33.4\,\mathrm{GeV}$) that arrived 82 seconds after the GBM trigger time, T_0. From the GBM light curves, we see that at energies $\lesssim 1\,\mathrm{MeV}$ the prompt phase ends approximately 25 seconds after T_0. Detailed analysis of the GBM data for energies 50–300 keV yields a formal T90 duration of 21.9 seconds starting at $T_0 + 2.2\,\mathrm{s}$. By contrast, the LAT emission >100 MeV clearly continues well after this time range.

On time scales longer than the prompt phase, the LAT detects emission from GRB 090902B as late as 1 ks after the GBM trigger. The spectrum of this emission is consistent with a power-law with photon index $\Gamma = -2.1 \pm 0.1$, and its flux (>100 MeV) declines as $\sim t^{-1.5}$ over the interval $(T_0 + 25, T_0 + 1000\,\mathrm{s})$. As we note above, the LAT observations are interrupted by entry of the Earth's limb into the FOV, but analysis of data after $T_0 + 3600\,\mathrm{s}$, when the source location is again unocculted, shows that any later emission lies below the LAT sensitivity (Figure 2). Similar late time emission for energies >100 MeV that extends well beyond the prompt phase has been seen for five earlier bursts by *Fermi*: GRB 080916C (Abdo et al. 2009d); GRB 090323 (Ohno et al. 2009); GRB 090328 (Cutini et al. 2009); GRB 090510, independently seen by AGILE (Giuliani et al. 2009) and by *Fermi* (Ghirlanda et al. 2009); and GRB 090626 (Piron et al. 2009).

4. Time-resolved Spectral Analysis

Spectral analysis was performed using the data from both the GBM and the LAT. These analyses include data from the NaI detectors 0,1,2,9,10 and both BGO detectors, and LAT "transient" class data, with front- and back-converting events considered separately. The NaI data are fit from 8 keV to 1 MeV and the BGO from 250 keV to 40 MeV using the Time Tagged Event (TTE) data type. The LAT data are fit from 100 MeV to 200 GeV. An effective area correction of 0.9 is applied to the BGO with respect to the NaI detectors and LAT for all fits. The fits were performed with the spectral analysis software package RMFIT (version 3.1). For further details on the data extraction and spectral analysis procedures see Abdo et al. (2009b) and Abdo et al. (2009c).

The time-integrated spectrum of GRB 090902B is best modeled by a Band function (Band et al. 1993) and a power-law component (Table 1). The power-law component, with

photon index Γ, significantly improves the fit between 8 keV and 200 GeV both in the time-integrated spectrum and in the individual time intervals where there are sufficient statistics. It is also required when considering only the GBM data (8 keV–40 MeV) for the time-integrated spectrum, as its inclusion causes an improvement of >1000 in the CSTAT statistic over the Band function alone. When data below ~ 50 keV are excluded, a power-law component can be neglected in the GBM-only fits. We therefore conclude that this power-law component contributes a significant part of the emission both at low (< 50 keV) and high (> 100 MeV) energies. Figure 3 shows the counts and unfolded νF_ν spectra for a Band function with a power-law component fit to the data for interval **b** (when the low energy excess is most significant) using the parameters given in Table 1.

Spectral evolution is apparent in the Band function component from the changing $E_{\rm peak}$ values throughout the burst, while β remains soft until interval **e** when it hardens significantly. β is similarly hard in interval **f**, after which the Band function component is no longer detected. The hardening of β is accompanied by an apparent hardening of the power-law index, Γ, which until interval **e** does not exhibit much variation. However, this is not definitive since the flux is too low to constrain Γ in intervals **e** and **f** separately. A spectral fit of the sum of these two intervals confirms the presence of both a harder β and a harder Γ, with a clear statistical preference for the inclusion of the power-law component. An equally good fit is obtained in the combined **e** + **f** interval if this power-law has an exponential cut-off at high energies, with the preferred cut-off energy lying above 2 GeV. Finally, we note that in interval **b**, a marginally better fit is achieved using a model with the additional power-law component having an exponential cut-off at high energies. The improvement is at the $\sim 3\sigma$ level and indicates weak evidence for a cutoff in the second component, placing a lower limit on the cutoff energy in this interval of about 1 GeV.

5. Discussion and Interpretation

The *Fermi* data for GRB 090902B show for the first time clear evidence of excess emission both at low energies ($\lesssim$ 50 keV) and at high energies (>100 MeV), while the Band function alone fits data at intermediate energies adequately. These excesses are well-fit by a single power-law component suggesting a common origin. This power-law component accounts for $\approx 24\%$ of the total fluence in the 10 keV–10 GeV range, and its photon index is hard, with a value ~ -1.9 throughout most of the prompt phase and may harden substantially in the final seconds. Such a hard component producing the observed excess at low energies is difficult to explain in the context of leptonic models by the usual synchrotron self-Compton (SSC) mechanisms (see, e.g., Piran 2005; Mészáros 2006).

In the simplest versions of these models, the peak of the SSC emission is expected to have a much higher energy than the synchrotron peak at MeV energies, and the SSC component has a soft tail that is well below the synchrotron flux at lower energies and so would not produce excess emission below $\sim$ 50 keV. Hadronic models, either in the form of proton synchrotron radiation (Razzaque et al. 2009) or photohadronic interactions (Asano et al. 2009), can produce a hard component with a similar low energy excess via direct and cascade radiation (e.g., synchrotron emission by secondary pairs at low energies). However, the total energy release in hadronic models would exceed the observed gamma-ray energy of $E_{\rm iso} = 3.63 \times 10^{54}$ ergs significantly and may pose a challenge for the total energy budget. Collimation into a narrow jet may alleviate the energy requirements, since the actual energy release from GRB 090902B can be smaller by a jet beaming factor $> 1/\Gamma_0^2$ from the apparent isotropic value, where Γ_0 is the bulk Lorentz factor of the fireball.

From the observation of a $11.16^{+1.48}_{-0.58}$ GeV photon in interval **c**, the highest energy during the prompt phase and thus the most constraining, we derive a minimum value of the bulk Lorentz factor $\Gamma_{\rm min} \approx 1000$ using the flux variability time scale of $t_v \approx 53$ ms found in the BGO data. This limit follows from the constraint that the opacity for $e^{\pm}$ pair production with target photons fitted by the Band+PL model in interval **c** is less than unity so that the 11.16 GeV photon can escape without attenuation (see, e.g., Fenimore et al. 1993; Woods & Loeb 1995; Baring & Harding 1997; Lithwick & Sari 2001). This high $\Gamma_{\rm min}$ value is of the same order as the values derived for GRB 080916C (Abdo et al. 2009d) and GRB 090510 (Abdo et al. 2009a), both of which have been detected at > 10 GeV with the LAT.

The delayed onset of the $\gtrsim$100 MeV emission from the GBM trigger has been modeled for GRB 080916C as arising from proton synchrotron radiation in the prompt phase (Razzaque et al. 2009) and for GRB 090510 as arising from electron synchrotron radiation in the early afterglow phase (Kumar & Barniol Duran 2009; Ghirlanda et al. 2009). In order to produce the peak of the LAT emission at $\sim T_0 + 9$ s in the early afterglow scenario for GRB 090902B from deceleration of the GRB fireball, a value of $\Gamma_0 \approx 1000$ is required. This is similar to $\Gamma_{\rm min}$ that we calculate, but the observed large amplitude variability on short time scales (≈ 90 ms) in the LAT data, which is usually attributed to prompt emission, argues against such models. Also, the appearance of the power-law component extending down to ≈ 8 keV within only a few seconds of the GRB trigger disfavors an afterglow interpretation. The proton synchrotron model, on the other hand, requires a rather large total energy budget, as mentioned previously.

Yet another interpretation of the observed excess in the high and low energies may be provided by two non-thermal power-law components along with a thermal component

from the jet photosphere (Mészáros & Rees 2000; Ryde 2004). The thermal component, broadened by temperature variations, then accounts for the $\gtrsim$ 100 keV–few MeV emission with $\Gamma_0 \approx 930$ (Pe'er et al. 2007), although fits of such a model to our data do not improve over the Band+PL model. Furthermore, it is difficult for the photospheric model to explain the delayed onset of the $\gtrsim 100$ MeV emission.

The detection of the 33.4 GeV photon, 82 seconds after the GRB trigger and well after the soft gamma-ray emission subsided, may help constrain the origin of the late-time decay of the power-law component, which goes as $t^{-1.5}$. A synchrotron origin of the 33.4 GeV photon would be difficult since it would require significant energy gain by electrons over a gyroradius and a bulk Lorentz factor > 600. In the case of diffusive shock-acceleration, the energy losses in the upstream region of the shock may dominate (see, e.g., Li & Waxman 2006) and prevent acceleration of electrons to an energy high enough to radiate a 33.4 GeV photon. An interpretation by afterglow SSC emission is still possible, however.

The constraints on the quantum gravity mass scale from GRB 090902B using the time-of-flight test (Amelino-Camelia et al. 1998) are much weaker than those from GRB 090510 (Abdo et al. 2009a) due to the larger interval, 82 seconds, between T_0 and the arrival time of the 33.4 GeV photon. However, the moderately high redshift ($z = 1.822$) of GRB 090902B allows us to use this photon to probe and constrain models of the Extragalactic Background Light (EBL; Kneiske et al. 2004; Metcalfe et al. 2003; Stecker et al. 2006; Franceschini et al. 2008; Gilmore et al. 2009; Finke et al. 2009). The 33.4 GeV photon would not be absorbed by the EBL in any models except for the "fast evolution" and the "baseline" models by Stecker et al. (2006), which give optical depths of $\tau_{\gamma\gamma} = 7.7$ and 5.8, respectively. We have performed spectral fits of the LAT data with and without the predicted EBL absorption from Stecker's models assuming a simple power-law as the intrinsic emission model. Based on Monte-Carlo simulations, we found that Stecker's fast evolution and baseline models are disfavored at a $> 3\sigma$ level.

In summary, GRB 090902B is one of the brightest bursts detected by the GBM and LAT instruments on *Fermi*. It clearly shows excess emission at high and low energies during the prompt phase, requiring a hard power-law component in addition to the usual Band function in order to fit the data. The origin of this component is not understood, and its presence in this burst poses some genuine challenges for the theoretical models. Like the other two bright *Fermi* bursts detected by the LAT, GRB 080916C and GRB 090510, GRB 090902B appears to possess a very high Lorentz factor for the bulk outflow, $\Gamma \approx 1000$, and has some suggestion of a delayed onset of the emission above ~ 100 MeV. Finally, the 33.4 GeV photon, the highest energy yet detected from a GRB, and the $z = 1.822$ redshift of this burst have allowed us to place significant constraints on some models of the Extragalactic Background

Light.

The *Fermi* LAT Collaboration acknowledges support from a number of agencies and institutes for both development and the operation of the LAT as well as scientific data analysis. These include NASA and DOE in the United States, CEA/Irfu and IN2P3/CNRS in France, ASI and INFN in Italy, MEXT, KEK, and JAXA in Japan, and the K. A. Wallenberg Foundation, the Swedish Research Council and the National Space Board in Sweden. Additional support from INAF in Italy and CNES in France for science analysis during the operations phase is also gratefully acknowledged.

REFERENCES

Abdo, A. A., et al. 2009a, Nature, submitted

—. 2009b, ApJ, submitted

—. 2009c, ApJ, in preparation

—. 2009d, Science, 323, 1688

Amelino-Camelia, G., Ellis, J., Mavromatos, N. E., Nanopoulos, D. V., & Sarkar, S. 1998, Nature, 395, 525

Asano, K., Guiriec, S., & Mészáros, P. 2009, ArXiv e-prints

Atwood, W. B., et al. 2009, ApJ, 697, 1071

Band, D., et al. 1993, ApJ, 413, 281

Baring, M. G., & Harding, A. K. 1997, ApJ, 491, 663

Bissaldi, E., & Connaughton, V. 2009, GCN, 9866

Chandra, P., & Frail, D. A. 2009, GCN, 9889

Cucchiara, A., Fox, D. B., Tanvir, N., & Berger, E. 2009, GCN, 9873

Cutini, S., Vasileiou, V., & Chiang, J. 2009, GRB Coordinates Network, 9077, 1

de Palma, F., Bregeon, J., & Tajima, H. 2009, GCN, 9867

Dingus, B. L., Catelli, J. R., & Schneid, E. J. 1998, in American Institute of Physics Conference Series, Vol. 428, Gamma-Ray Bursts, 4th Hunstville Symposium, ed. C. A. Meegan, R. D. Preece, & T. M. Koshut, 349–353

Fenimore, E. E., Epstein, R. I., & Ho, C. 1993, A&AS, 97, 59

Finke, J. D., Razzaque, S., & Dermer, C. D. 2009, ArXiv e-prints

Franceschini, A., Rodighiero, G., & Vaccari, M. 2008, A&A, 487, 837

Gehrels, N., et al. 2004, ApJ, 611, 1005

Ghirlanda, G., Ghisellini, G., & Nava, L. 2009, ArXiv e-prints

Gilmore, R. C., Madau, P., Primack, J. R., Somerville, R. S., & Haardt, F. 2009, ArXiv e-prints

Giuliani, A., et al. 2008, A&A, 491, L25

—. 2009, ArXiv e-prints

González, M. M., Dingus, B. L., Kaneko, Y., Preece, R. D., Dermer, C. D., & Briggs, M. S. 2003, Nature, 424, 749

Greiner, J., et al. 2009, A&A, 498, 89

Guidorzi, C., Tanvir, N. R., Cano, Z., Steele, I. A., Bersier, D., et al. 2009, GCN, 9875

Hurley, K., et al. 1994, Nature, 372, 652

Kaneko, Y., González, M. M., Preece, R. D., Dingus, B. L., & Briggs, M. S. 2008, ApJ, 677, 1168

Kennea, J., & Stratta, G. 2009, GCN, 9868

Kneiske, T. M., Bretz, T., Mannheim, K., & Hartmann, D. H. 2004, A&A, 413, 807

Kumar, P., & Barniol Duran, R. 2009, ArXiv e-prints

Li, Z., & Waxman, E. 2006, ApJ, 651, 328

Lithwick, Y., & Sari, R. 2001, ApJ, 555, 540

Meegan, C., Lichti, G., Bhat, P. N., Bissaldi, E., Briggs, M. S., et al. 2009, ApJ In Press

Mészáros, P. 2006, Reports on Progress in Physics, 69, 2259

Mészáros, P., & Rees, M. J. 2000, ApJ, 530, 292

Metcalfe, L., et al. 2003, A&A, 407, 791

Ohno, M., Cutini, S., McEnery, J., Chiang, J., & Koerding, E. 2009, GRB Coordinates Network, 9021, 1

Olivares, F., Afonso, F., Greiner, J., McBreen, S., Kruehler, T., Rau, A., Yoldas, A., & G., K. 2009, GCN, 9874

Pandey, S. B., Zheng, W., Yuan, F., & Akerlof, C. 2009, GCN, 9878

Pe'er, A., Ryde, F., Wijers, R. A. M. J., Mészáros, P., & Rees, M. J. 2007, ApJ, 664, L1

Perley, D., Kleiser, I. K. W., & Rex, J. M. 2009, GCN, 9870

Piran, T. 2005, Reviews of Modern Physics, 76, 1143

Piron, F., Longo, F., Iafrate, G., Cheung, T., Tajima, H., & Connaughton, V. 2009, GRB Coordinates Network, 9584, 1

Rau, A., McBreen, S., Kruehler, T., & Greiner, J. 2009, GCN, 9353

Razzaque, S., Dermer, C. D., & Finke, J. D. 2009, ArXiv e-prints

Rossi, A., et al. 2008, A&A, 491, L29

Ryde, F. 2004, ApJ, 614, 827

Stecker, F. W., Malkan, M. A., & Scully, S. T. 2006, ApJ, 648, 774

Stratta, G., D'Elia, V., & Perri, M. 2009, GCN, 9876

Swenson, C. A., & Siegel, M. H. 2009, GCN, 9869

Swenson, C. A., & Stratta, G. 2009, GCN, 9877

Terada, Y., et al. 2009, GCN, 9897

van der Horst , A. J., Kamble, A. P., Wijers, R. A. M. J., & Kouveliotou, C. 2009, GCN, 9883

Woods, E., & Loeb, A. 1995, ApJ, 453, 583

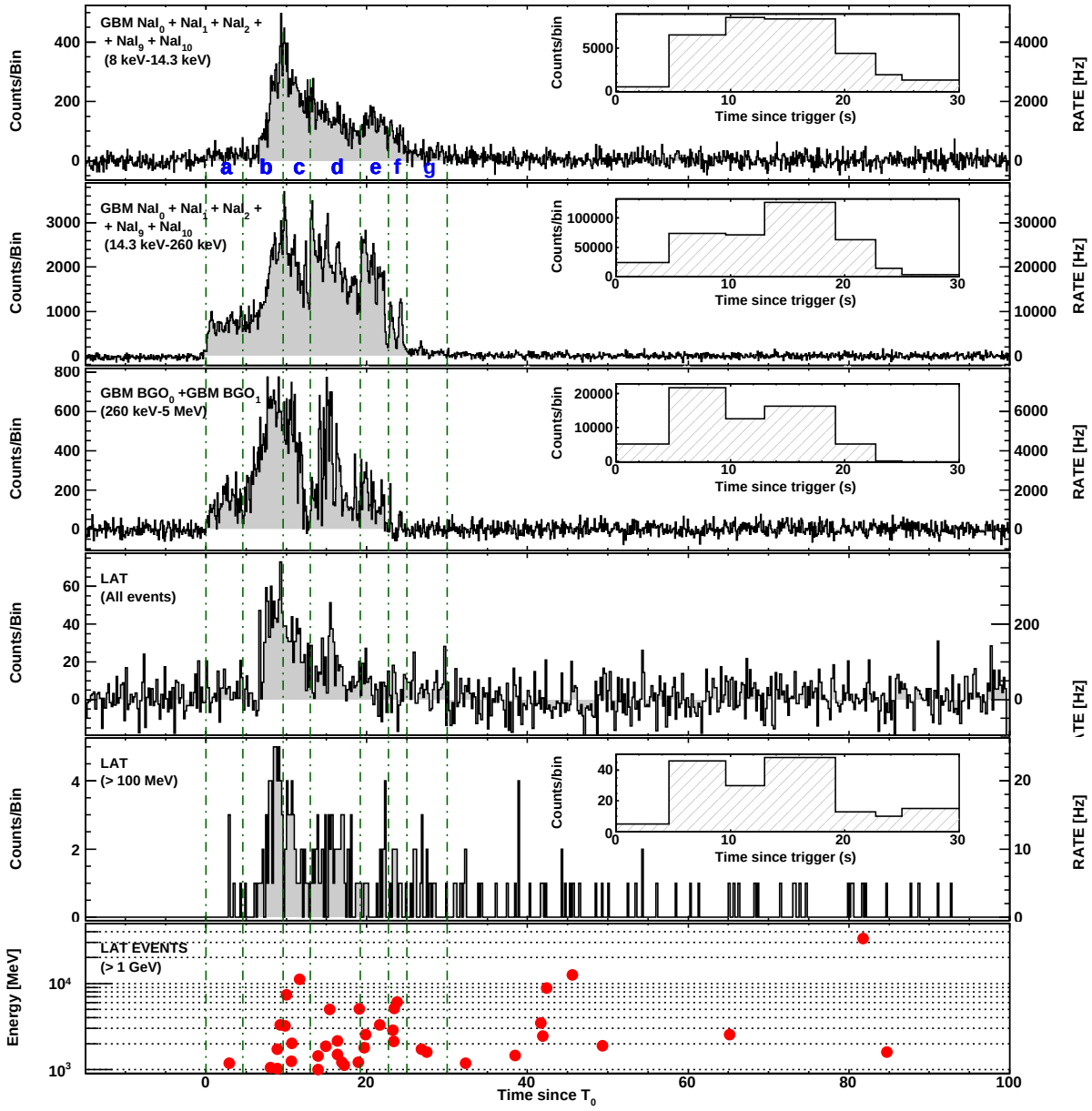

Fig. 1.— GBM and LAT light curves for the gamma-ray emission of GRB 090902B. The data from the GBM NaI detectors were divided into soft (8–14.3 keV) and hard (14.3–260 keV) bands in order to reveal any obvious similarities between the light curve at the lowest energies and that of the LAT data. The fourth panel shows all LAT events that pass the on-board gamma filter, while the fifth and sixth panels show data for the "transient" class event selection for energies $> 100\,\mathrm{MeV}$ and $> 1\,\mathrm{GeV}$, respectively. The vertical lines indicate the boundaries of the intervals used for the time-resolved spectral analysis. Those time boundaries are at $T_0 + (0, 4.6, 9.6, 13.0, 19.2, 22.7, 25.0, 30.0)$ seconds. The insets show the counts for the corresponding dataset binned using these intervals in order to illustrate the relative numbers of counts considered in each spectral fit.

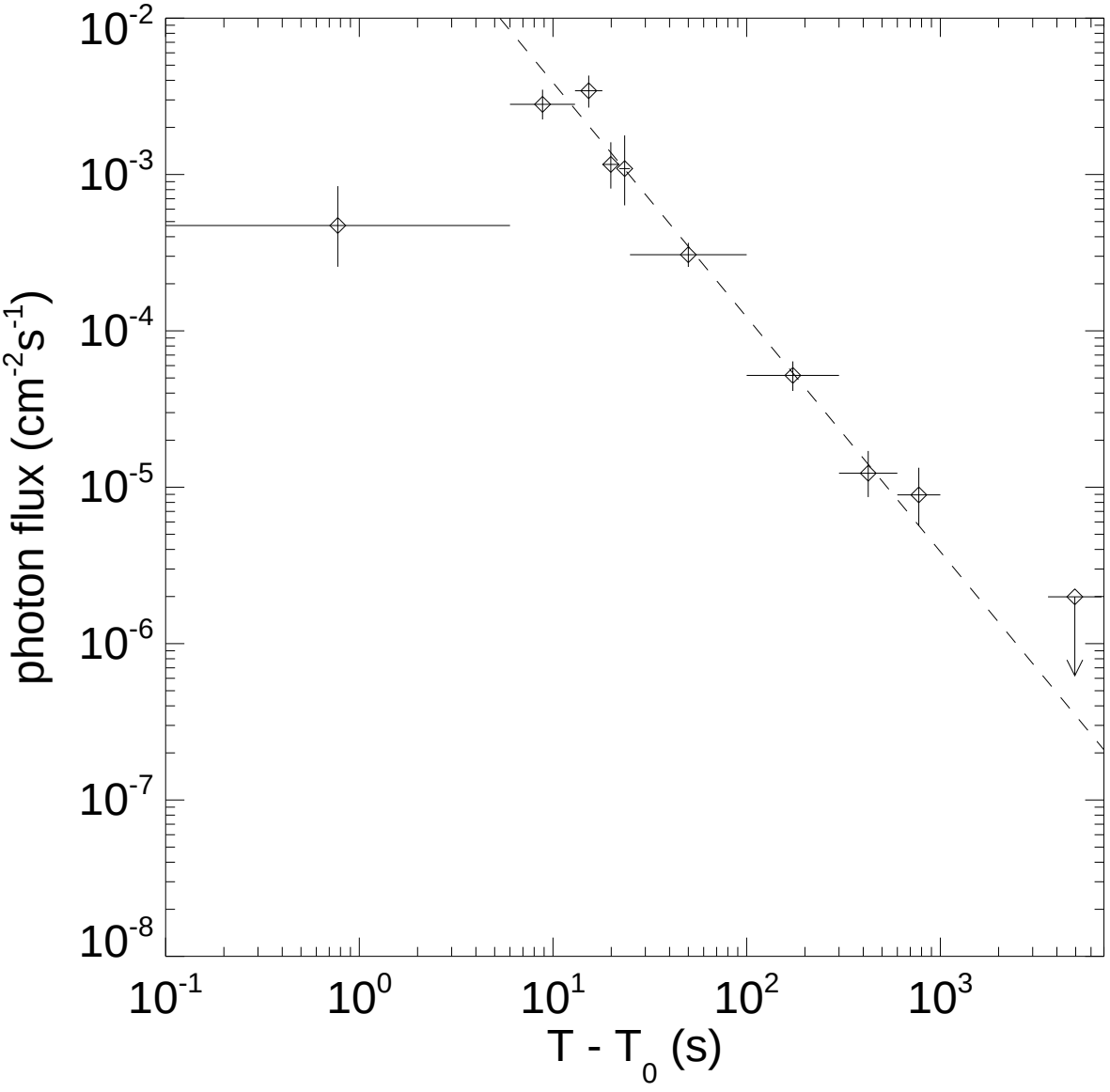

Fig. 2.— Light curve of GRB 090902B for energies 0.1–300 GeV from unbinned likelihood fits to the LAT data. After the prompt phase, extended or afterglow emission consistent with a temporal profile $\propto t^{-1.5}$ lasts until $\sim T_0 + 1000\,\mathrm{s}$. A dashed line with this dependence is plotted to guide the eye. The upper limit at times $> T_0 + 3600\,\mathrm{s}$ was derived from the data collected after the source emerged from occultation by the Earth.

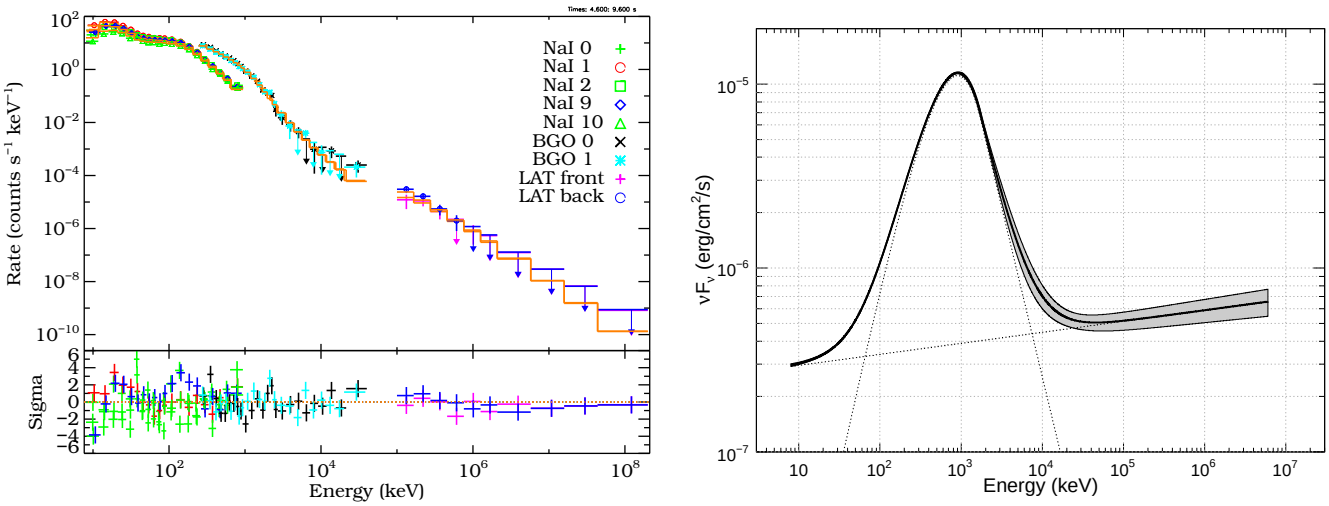

Fig. 3.— Joint fit of GBM and LAT data to interval **b**, $(T_0+4.6, T_0+9.6\,\mathrm{s})$ Left: counts spectrum; right: unfolded νF_ν spectrum. The extension of the $> 100\,\mathrm{MeV}$ power-law component to the lowest energies ($< 50\,\mathrm{keV}$) is shown.

Table 1. Band function + power-law fit parameters for the time-resolved spectral fits.

Interval	Time Range (s)	E_{peak} (kev)	α	β	Γ	CSTAT/DOF	Energy fluence ($erg\,cm^{-2}$, 8 keV–30 GeV)
···	0.0–30.0	726 (±8)	-0.61 (±0.01)	-3.8 $(^{+0.2}_{-0.3})$	-1.93$(^{+0.01}_{-0.01})$	2562/963	$(4.59 \pm 0.05)\times10^{-4}$
a.	0.0–4.6	526 (±12)	-0.09 (±0.04)	-3.7 $(^{+0.3}_{-0.6})$	-1.87$(^{+0.04}_{-0.05})$	901/964	$(3.72 \pm 0.13)\times10^{-5}$
b.	4.6– 9.6	908 $(^{+15}_{-14})$	0.07 (±0.03)	-3.9 $(^{+0.2}_{-0.3})$	-1.94 (±0.02)	1250/963	$(1.44 \pm 0.03)\times10^{-4}$
c.	9.6–13.0	821 (±16)	-0.26 (±0.03)	-5.0$(^{+0.8}_{-\infty})$	-1.98 (±0.02)	1310/963	$(9.42 \pm 0.24)\times10^{-5}$
d.	13.0–19.2	529 (±9)	-0.65 (±-0.02)	-3.2 $(^{+0.1}_{-0.2})$	-1.86 (± 0.02)	1418/963	$(1.29 \pm 0.03)\times10^{-4}$
e.	19.2–22.7	317 (±8)	-0.78 (±-0.02)	-2.4 (±0.1)	···	1117/965	$(4.8 \pm 0.2) \times10^{-5}$
f.	22.7–25.0	236 $(^{+25}_{-33})$	-1.30 $(^{+0.04}_{-0.03})$	-2.2 (±0.1)	···	1077/965	$(1.0 \pm 0.1)\times10^{-5}$
e.+f.	19.2–25.0	327 (±8)	-0.91±0.02	-2.6±0.1	-1.59±0.2	1219/963	$(6.1 \pm 0.4)\times10^{-5}$
g.	25.0–30.0	···	···	···	-1.93 $(^{+0.25}_{-0.26})$	1209/967	$(6.8 \pm 0.8)\times10^{-6}$

Note. — The time range values are relative to the trigger time T_0. Combining intervals **e** and **f** increases the statistics and is well fit by the Band function plus a power-law component.